

# Solidification Behavior Study of Al-8 wt% Mg Alloy

Afaf Djarouï<sup>1</sup>, Samia Nebti<sup>2</sup>

<sup>1</sup>Département Sciences et Techniques, Faculté de Technologie, Université Batna2, Batna, Algérie

<sup>2</sup>Département de Physique, Faculté des Sciences Exactes, Université Mentouri, Constantine, Algérie

Keywords: Binary alloy, Fluent, Solidification, Simulation.

Abstract: We consider a 2D numeric simulation of the liquid-solid transition in an Al-Mg alloy. The liquid melt is contained in an axisymmetric rectangular enclosure with isothermal walls. The heat transfer is modelled using the Fluent V.6.3.26 code. In the unsteady state of the process, free convective fluid flows are seen as two contra-rotating swirls. This movement is driven by the important temperature gradients generated in the liquid region. When the steady state is established (liquid-solid equilibrium), the velocities determining the convective flows are cancelled. The solidification proceeds then by a purely conductive mode. The interface shape is determined during the unsteady state by the convective flows, and then, remains unchanged until the solidification process is achieved.

## 1 INTRODUCTION

The numerical modelling of alloy solidification is still a formidable task to simulate the transport of heat and solute. Alloy's solidification is a complicated process given that the influence of different parameters governing the solidification problem (Djarouï, 2016), (AsleZaem, 2012), (Djarouï, 2009), (Zhu, 2007), (Betram-Sanchez, 2004), (McFadden, 2000), (Glicksman, 1994), (Trivedi, 1994), (Trivedi, 1990), (Ben Amar, 1989), (Meiron, 1986). The convection phenomenon manifesting in the melt and mushy region is the most important factor seen its controlling the shape, extent and advancement of the mushy zone. The most common causes of fluid flow in the solidification process are thermal and solutal gradients, surface tension gradients and external forcing agents. Natural convection can influence the advancement of the solidification front even in highly conductive alloys.

The purpose of this work is to predict the solidification evolution under thermal condition and the role of convective transfer in a highly conductive binary alloy. A finite volume analysis is carried out by the Fluent V.6.3.26 code for a two dimensional enclosure in the unsteady state stage.

## 2 PROBLEM FORMULATION

### 2.1 Fundamentals Equations

Solidification is a process in which a solid grows from a liquid. The treatment of this phase change using Fluent is done considering an enthalpy-porosity technique. The domain is divided into three regions (liquid, solid and the mushy zone), a liquid fraction value  $f_L$  is associated with each cell in the domain (0 for liquid, 1 for the solid and lie between 0 and 1 for the mushy zone). The melt – solid interface is not tracked explicitly (Fluent® 6.2 User's Guide), (Conde, 2004).

The equations used to solve the alloy solidification problem are:

The energy equation:

$$h = h_{ref} + \int_{T_{ref}}^T c_p dT \quad (1)$$

Where  $h$  is the enthalpy,  $h_{ref}$  is the reference enthalpy,  $T_{ref}$  is the reference temperature and  $c_p$  is the specific heat capacity at constant pressure.

The liquid fraction, ( $f_L$ ) equation:

$$f_L = \begin{cases} 1 & T > T_{liq} \\ \frac{(T - T_{sol})}{(T_{liq} - T_{sol})} & T_{sol} < T < T_{liq} \\ 0 & T < T_{sol} \end{cases} \quad (2)$$

Where  $T_{liq}$ ,  $T_{sol}$ ,  $T$  are liquidus, solidus and mushy zone temperatures respectively.

The energy conservation equation:

$$\frac{\partial}{\partial t}(\rho h + \rho f_L L_v) + \nabla(\rho \vec{v} h) = K \Delta T \quad (3)$$

Where  $\rho$  is the density,  $\vec{v}$  is the fluid velocity,  $L_v$  is the latent heat of fusion and  $K$  is the thermal conductivity.

## 2.2 Boundary Condition

The simulation, which has been carried out with the Fluent<sup>®</sup> v6.3.26 code, is applied to the Al-Mg alloy. The alloy liquid is contained in a 2D enclosure of  $L=0.1\text{m}$  height and  $D=0.01\text{m}$  width as presented in Figure. 1. The calculation was optimized in order to ensure an independence of the results with respect to the grid. In order to allow the solidification, a temperature  $T_w=815\text{K}$  lower than the solidus temperature of the fluid ( $T_{sol}$ ), is assigned to the walls of the enclosure. In order to study the temperature difference ( $\Delta T=T_0-T_w$ ) effect on the convective flow, we attributed different values to the initial fluid temperature  $T_0$  ( $820\text{K} \leq T_0 \leq 915\text{K}$ ). The symmetry of the problem (horizontal and vertical) reduces the computational domain to the 1/4 of the total volume. The properties of the liquid melt using are given in table.1.

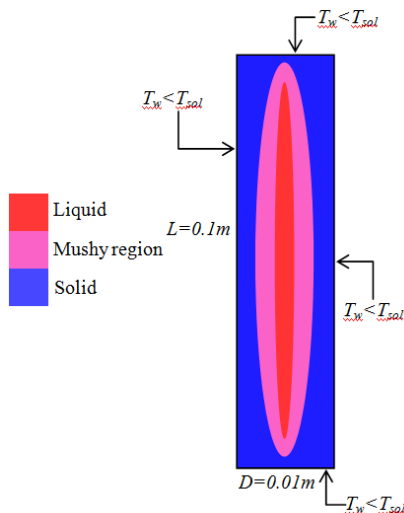


Figure 1. Scheme of the geometrical model.

Table.1. Thermal properties of the Al-8%Mg liquid alloy used in the calculation.

Thermal properties	Symbol	Units	value
Density	$\rho$	$\text{Kg/m}^3$	2623.2
Specific heat	$c_p$	$\text{J/Kg.K}$	1085,608
Latent heat	$L_v$	$\text{KJ/Kg}$	404
Thermal conductivity	$K$	$\text{W/m.K}$	221,36
Viscosity	$\mu$	$\text{Kg/m.s}$	0,0013
Thermal expansion coefficient	$\beta_T$	$\text{K}^{-1}$	$2,67 \cdot 10^{-5}$
Solidus temperature	$T_{sol}$	K	819.82
Liquidus temperature	$T_{liq}$	K	893.15

## 3 RESULTS AND DISCUSSION

### 3.1 $\Delta T$ Effect on the Solidification Evolution

Considering different values of  $\Delta T$  in the solidification modelling using Fluent gives us the results represented in table.2 where  $t_1$  is the time where the unsteady state stage is achieved and  $t_2$  represents the time of the end of the solidification process.

Table2: Temperature difference effect on the time

$\Delta T(\text{K})$	$t_1(\text{s})$	$t_2(\text{s})$
5	/	0.071
10	/	0.653
20	/	1.205
30	0.244	1.531
50	0.543	1.932
70	0.761	2.201
100	0.853	2.312

It is noted that at the beginning of the solidification process, significant  $\Delta T$  values ( $\Delta T \geq 30\text{K}$ ) create a convective movement of the liquid melt, in the grid plane, as two contra-rotating swirls symmetrically to the vertical axis as it is illustrated in figure.2. The steady state is established very quickly. For the lower  $\Delta T$  values ( $\Delta T < 30\text{K}$ ) we note the absence of the unsteady state stage.

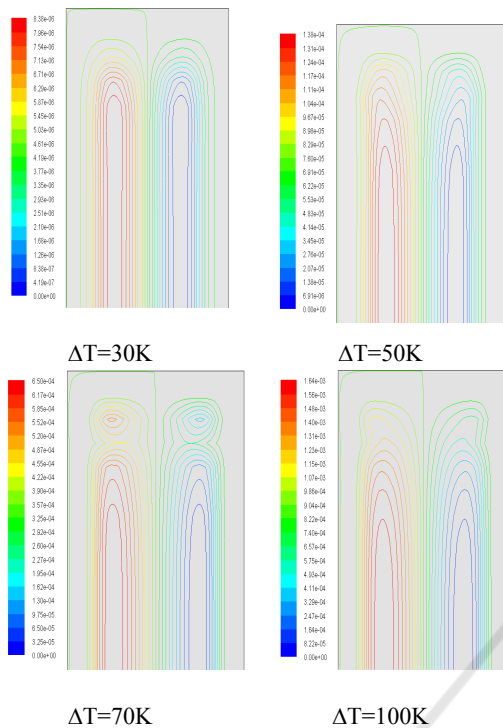


Figure 2. Contours of stream function (Kg/s) at  $t = 0.1s$  for different values of  $\Delta T$ .

### 3.2 Fluid Flow

The development of buoyancy forces in the enclosure plane, due to the temperature gradients, produces a natural convection movement. The presented flow fields are at time  $t=0.1s$ . As exposed in figure 2, the hot fluid is guided upwards and once reaching the cold wall, the flow is separated into two parts deviated on the right and on the left in a movement downwards symmetrically to the vertical axis. The two flow parts meet at the bottom of the enclosure in an ascending movement giving two swirls contra-rotating, in the enclosure plan, separated by the symmetry axis. In the  $\Delta T=70K$  case, each of the two vortices is divided into three parts: two small vortices (close to horizontal walls) and a main vortex between them. Within the small vortices, flow particles cannot follow the accelerated motion of the main vortex along the vertical wall and they are deviated towards the middle of the enclosure. This deviation may be explained by the weak momentum of the fluid particles within the small vortices. However, for  $\Delta T=100K$ , at the specified time, the flow field is represented by the two swirls contra-rotating, in the plan of the enclosure, and we notice the absence of the small

swirls. At this time, the mentioned small vortices have already merged with the main swirls because of the faded motion of the main swirls.

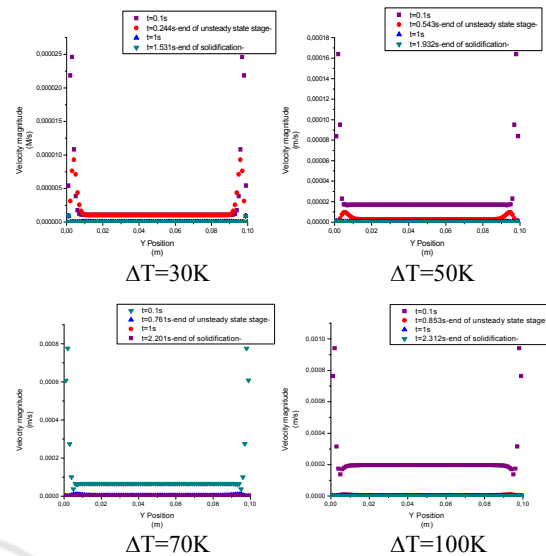


Figure 3. Velocity magnitude curves for different  $\Delta T$  values.

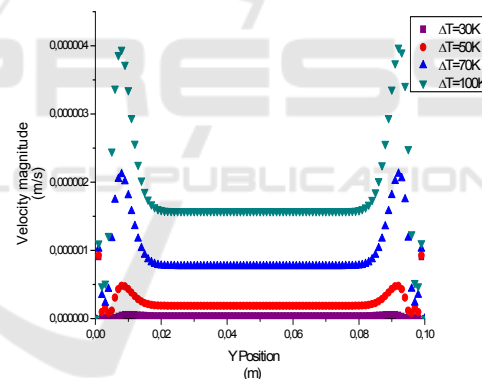


Figure 4. Velocity magnitude curves for different  $\Delta T$  values at the vertical axis ( $x=0.005m$ ) at  $t=1s$ .

Figures 3 and 4 indicate that the important temperature difference ( $\Delta T=100K$ ) has the maximal magnitude velocity and so generates an important convective movement of the liquid melt.

As it is shown in figure 5, the velocity is maximal ( $v = 3.510^{-6}m/s$ ) for  $y=0.01m$  and  $y=0.09m$  (near the walls) and constant for each other  $y$ . The velocity is maximal for  $x=0.05m$  and it decreases for each other  $x$  points, which indicates that important convective current results in the enclosure centre.

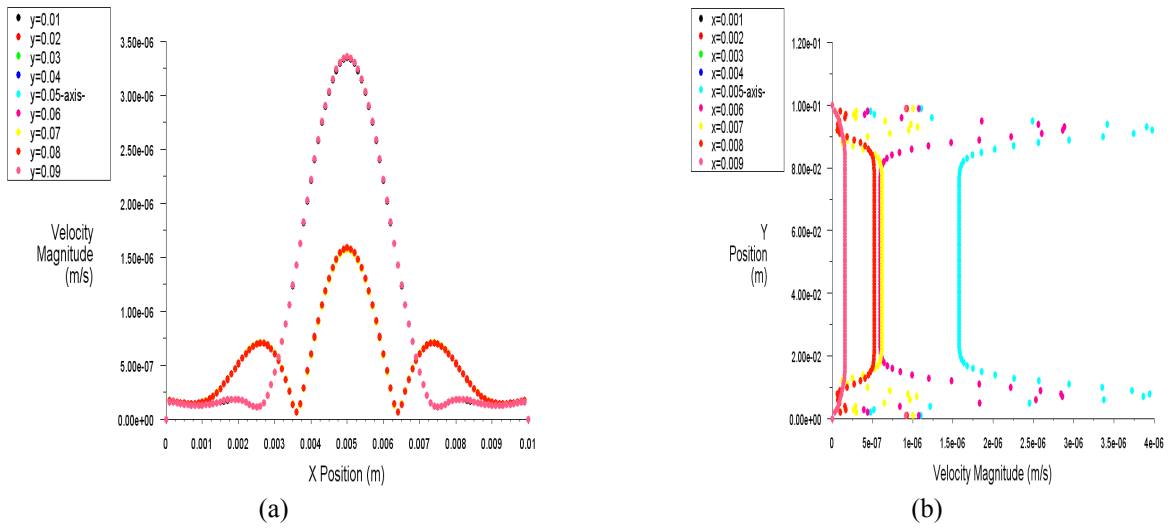


Figure 5. Velocity magnitude for  $\Delta T=100K$  at  $t=1s$ .

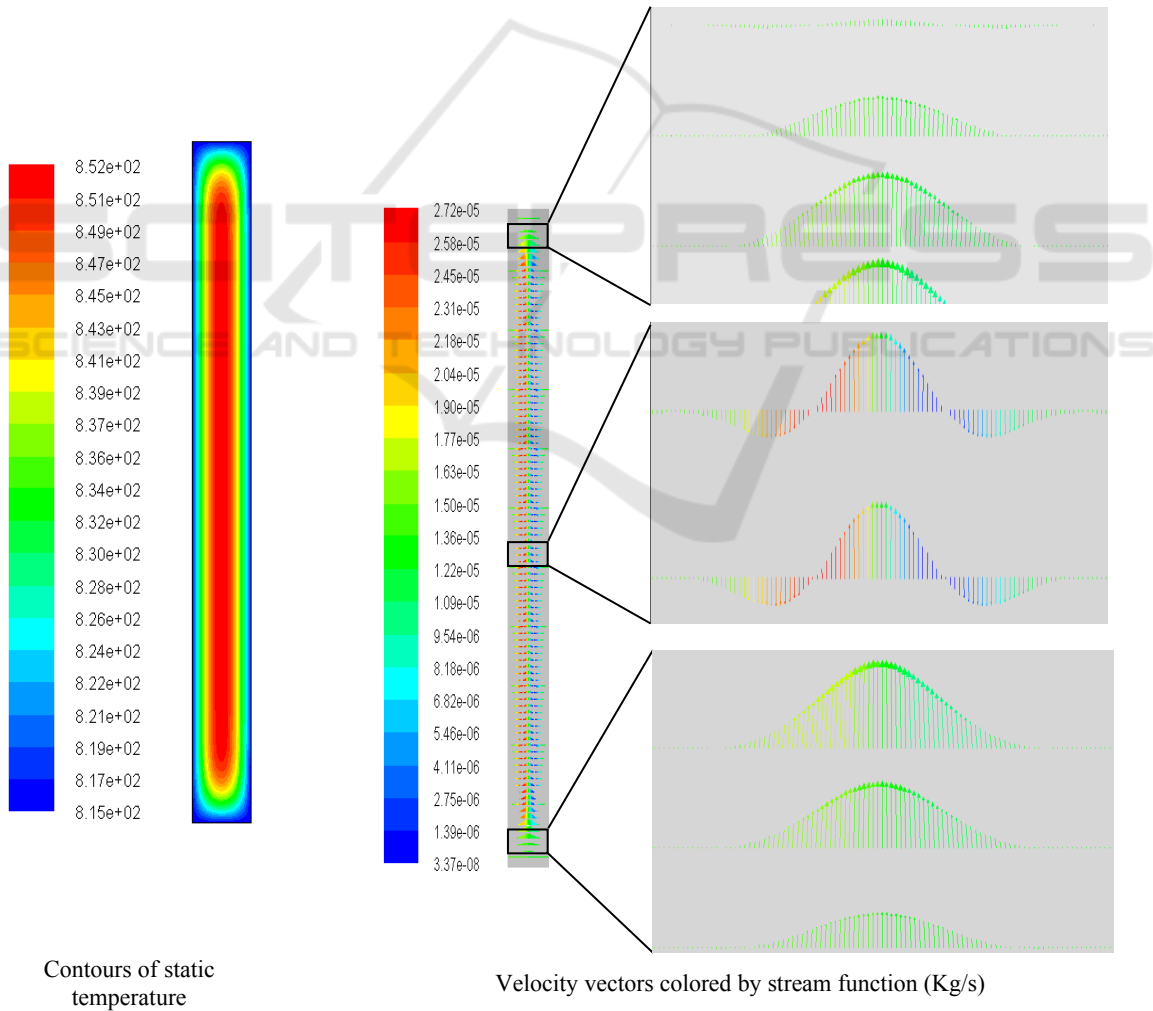


Figure 6. Temperature difference effect on the convective movement at  $t=0.8s$  (before the end of the unsteady state stage) for  $\Delta T=100K$ .

Figure.6 illustrates that the liquid flow depends on the temperature gradient: Near the up and the down walls the convective movement flow one direction. In the geometry centre, the liquid flow is governed by the density variations which is strongly influenced by the temperature gradients

### 3.3 Temperature Field

The temperature differences implicate the generation of the driving thermal force, which provokes a natural convection movement. The hot liquid is driven upwards and once reaching the cold wall, it is separated into two parts by the vertical symmetry axis. In the bottom, the two parts meet in an upswing thus creating two vortices contra-rotating divided by the vertical symmetry axis. This phenomenon is illustrated in figure.7 (contours of static temperature).

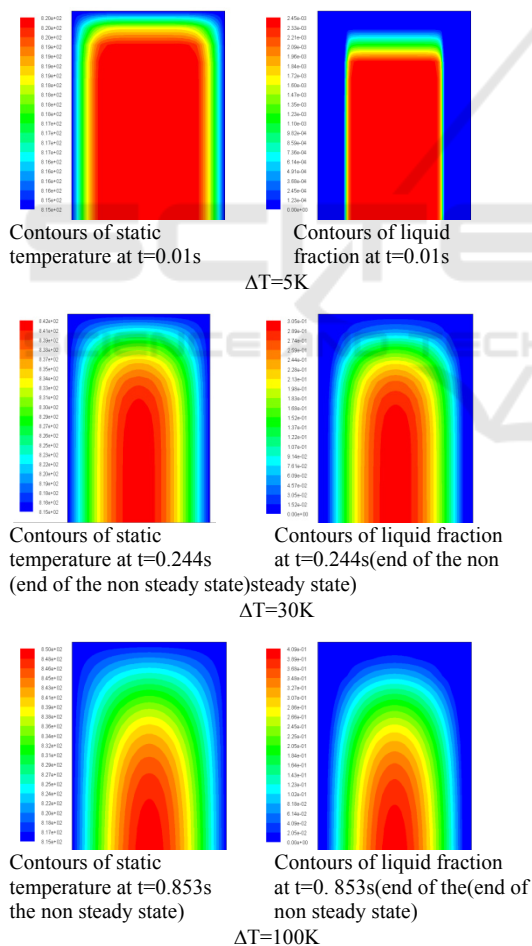


Figure 7. Contours of static temperature and liquid fraction.

### 3.4 Liquid Fraction

Looking at the contours of liquid fraction representing in Figure. 7, we can assume that the same behaviour, detecting for the temperature contours, is observed for the contours of liquid fraction

## 4 CONCLUSION

During the solidification process, the motion of the Al-Mg liquid melt is initially driven by the temperature gradients. An unsteady state stage appears for important values of temperature differences between the walls and the liquid alloy temperatures ( $\Delta T \geq 30K$ ). Free convective fluid flows are generated as two contra-rotating swirls. For  $\Delta T=70K$ , the two contrarotative swirls are divided into three parts. Two satellites are created, limiting a central swirl, in the upwards and the downwards of the enclosure. When the steady state is established (liquid-solid equilibrium), the velocities determining the convective flows are cancelled. The solidification proceeds then by a purely conductive mode. The interface shape is determined during the unsteady state stage by the convective flows, and then, remains unchanged until the solidification process is achieved.

## REFERENCES

- Djaraoui, A., & Nebti, S. (2016). On the Origin of Grid Anisotropy in the Simulation of Dendrite Growth by a VFT Model. *Metallurgical and Materials Transactions A*, 47(10), 5181-5194.
- Zaem, M. A., Yin, H., & Felicelli, S. D. (2012). Comparison of cellular automaton and phase field models to simulate dendrite growth in hexagonal crystals. *Journal of Materials Science & Technology*, 28(2), 137-146.
- Djaraoui, A., Nebti, S., Noui, S., (2009). Analysis of no-steady state stage during rapid solidification of an Al-Mg alloy, 9ème Congrès de Mécanique, FS Semlalia, Marrakech.
- Zhu, M. F., & Stefanescu, D. M. (2007). Virtual front tracking model for the quantitative modeling of dendritic growth in solidification of alloys. *Acta Materialia*, 55(5), 1741-1755.
- Zhu, M. F., Stefanescu, D. M., 2007. Virtual front tracking model for the quantitative modeling of dendritic growth in solidification of alloys, *Acta Materialia*, 55: 1741-1755,.

- Beltran-Sanchez, L., & Stefanescu, D. M. (2004). A quantitative dendrite growth model and analysis of stability concepts. *Metallurgical and Materials Transactions A*, 35(8), 2471-2485.
- Conde, R., Parra, M. T., Castro, F., Villafruela, J. M., Rodríguez, M. A., & Méndez, C. (2004). Numerical model for two-phase solidification problem in a pipe. *Applied thermal engineering*, 24(17-18), 2501-2509.
- McFadden, G. B., Coriell, S. R., & Sekerka, R. F. (2000). Effect of surface free energy anisotropy on dendrite tip shape. *Acta materialia*, 48(12), 3177-3181.
- Glicksman, M. E., Koss, M. B., & Winsa, E. A. (1994). Dendritic growth velocities in microgravity. *Physical review letters*, 73(4), 573.
- Trivedi, R. K., Kurz, W. (1994). Dendritic growth. *International Materials Review*, 39: 49-74.
- Trivedi, R. K., Mason, J. T. (1990). The effect of interface kinetics on solidification interface morphologies. *Metallurgical Transactions A*, 21, 235-249.
- Ben Amar, M., Pelce, P. (1989). Impurity effect on dendritic growth. *Phys rev A*, 39, 4263.
- Meiron, D. I. (1986). Selection of steady states in the two-dimensional symmetric model of dendritic growth. *Phys Rev A*, 33, 2704.
- Fluent® 6.2 User's Guide.

